Plasma Flow Control on a Landing Gear Model

Michael Wicks[1], Flint O. Thomas[2], and Thomas C. Corke[3]
Aerospace & Mechanical Engineering Department
University of Notre Dame,
Notre Dame, IN, 46556

Chris Nelson[4], Mehul Patel[5], and Alan B. Cain[6]
Innovative Technology Applications Company, LLC
14929 Royalbrook Dr
Chesterfield, MO 63017-7722

This paper reports an effort to extend bluff-body plasma noise control technology demonstrated for a tandem cylinder configuration in [28,29] to a realistic landing gear geometry. Experiments and numerical simulations are presented which focus on plasma flow control of a generalized tandem geometry consisting of the interaction between the hydraulic strut and downstream torque arm of the Gulfstream G550 nose landing gear. Experiments and numerical simulations are preformed at a Re_D = 122,000 and M = 0.081. This component work is considered prerequisite to the broader goal of demonstrating plasma noise control on a partially dressed, closed cavity 30% scale model of a Gulfstream G550 nose gear.

Nomenclature

Cp_{rms}	=	root-mean-square pressure coefficient
U_∞	=	free-stream velocity
St_D	=	Strouhal number with respect to leading cylinder diameter
Re_D	=	Reynolds number with respect to leading cylinder diameter
L	=	center-to-center distance from cylinder to face of torque arm
D	=	leading cylinder diameter
FAC	=	cutoff frequency
k	=	wavenumber
k_{cut}	=	cutoff wavenumber
P_{ref}	=	static pressure
ρ_{ref}	=	static fluid density
V_{ref}	=	reference velocity

I. Introduction

Projected increases in civil air traffic, coupled with a larger population in the vicinity of major airports will result in increased community noise impact. This, in turn, will result in continued pressure to reduce aircraft noise on take-off and landing. Aircraft noise will remain a major constraint on the growth of the commercial air transportation system unless new technologies can be developed to reduce community noise impact.

It is well known the jet noise component of overall aircraft noise has been significantly reduced by the utilization of quieter, high-bypass ratio engines. In envisioned blended wing body (BWB) subsonic transport designs, the engines are located on the upper surface of the aircraft and so engine exhaust noise is not reflected downward by the lower surface of the wing. In landing approach, when engines are throttled down, airframe noise

---

[1] Research Assistant, Department of Aerospace and Mechanical Engineering, Center for Flow Physics and Control, Student Member.
[2] Professor, Department of Aerospace and Mechanical Engineering, Center for Flow Physics and Control, Associate Fellow.
[3] Professor, Department of Aerospace and Mechanical Engineering, Center for Flow Physics and Control, Fellow.
[4] Chief Scientist, Computational Fluid Dynamics, Innovative Technology Applications Company, LLC.
[5] Vice President, Advanced Programs, Innovative Technology Applications Company, LLC.
[6] President, Innovative Technology Applications Company, LLC.

now represents a primary noise source for existing subsonic commercial transports and is comparable to the jet noise component. This will continue to be a problem for future designs as well. This has spawned considerable interest in understanding the physical mechanisms responsible for airframe noise production and how they can be predicted and controlled. A combination of experimental and computational airframe noise research has identified key sources of airframe noise that appear more or less generic to the current generation of commercial transport aircraft. These include: (1) landing gear noise (associated with flow past landing gear main and nose wheels, oleo legs and struts, uncovered wheel wells, doors and other undercarriage elements) and (2) high-lift system noise associated with trailing flaps, leading edge slats and the associated brackets and rigging. While the BWB has no slotted trailing edge flaps, designs include simple hinged trailing edge flaps (that double as elevons), a leading edge slat and landing gear so that these noise sources certainly remain relevant. The detailed physical mechanisms of noise production from these sources are still a topic of active investigation. However, it is clear that a common feature of each is a region of unsteady, separated flow. The relative magnitude of these noise sources is configuration dependent but all generally have comparable amplitudes (although the noise peaks typically occur at different frequencies). The noise from each source adds logarithmically to contribute to the overall sound pressure level (OASPL). As shown in [1], this clearly implies that to achieve stated NASA noise reduction goals, one must reduce each of the contributing airframe noise sources by the same amount. As a first step in this process of integrated airframe noise reduction, consideration is given to landing gear noise control by active means.

A. Landing Gear Noise

Flyover tests have shown that landing gear noise represents a primary source of airframe noise [2]. The inherent bluff body characteristics of landing gear give rise to large-scale flow separation that results in noise production through unsteady wake flow and large-scale vortex instability and deformation [3]. Large-scale, unsteady Reynolds-averaged Navier-Stokes simulations of the flow field over a landing gear assembly have been performed which capture the unsteady vortex shedding that occurs from the oleo and struts as well as from the landing gear box and rear wheels [4]. This study also serves to demonstrate the extreme complexity of the unsteady flow over the gear. Since the landing gear components encompass a wide range of sizes, the noise associated with shedding from the gear is broadband in nature with the peak in the spectrum occurring around a few hundred Hertz. A full, aeroacoustic analysis of a landing gear assembly was reported by Lockard, Khorrami and Li [5]. Data from an unsteady Reynolds Averaged Navier-Stokes simulation of the flow over a landing gear assembly was used as input to the Ffowcs Williams-Hawking equation in order to predict the noise at far-field observer locations. These computations demonstrate the potential of large-scale numerical simulations in the identification of acoustic sources in complex landing gear geometries. Fundamental work has considered the unsteady flow and noise generated by generic geometries relevant to landing gear like tandem cylinders in cross-flow [6-10]. Steady and unsteady wake surveys of a fully extended A340 center landing gear model were presented in [11]. An aeroacoustic study was conducted on a 26%-scale Boeing 777 main landing gear in the Virginia Tech (VT) Anechoic Stability Wind Tunnel [12]. Four types of passive flow control in the form of strut and brace fairings, a lower truck faring and the NASA toboggan geometry were investigated to determine their effectiveness in landing gear noise reduction. In addition to the use of mechanical fairings, removal of small gear parts like hydraulic lines, nuts and tubes has been shown to reduce the high frequency portion of gear noise [13, 14]. Although removal is not practical, smaller parts could be hidden behind larger elements or stowed in dead flow regions. Passive flow control in the form of fairings that are designed to reduce flow separation over landing gear elements have the advantage that they reduce the landing gear noise over the entire spectrum, especially the peak low frequency region. However, their use in real aircraft may be limited by practical considerations like the need to allow easy access for gear maintenance and the ability to stow the gear in cruise.

In a partnership between NASA and Gulfstream, a 25% scale model of a Gulfstream G550 nose gear was studied in the BART wind tunnel facility at NASA Langley Research Center in order to characterize the aerodynamic interactions between multiple gear components that likely play a key role in landing gear noise generation [15]. Both static and unsteady surface pressures were measured at numerous locations. The surface pressure spectra were broadband which is consistent with complementary PIV wake surveys that showed the wake flow field to be a complex collection of separated shear layers without any dominant vortex shedding processes. Acoustic noise source measurements on the 25% Gulfstream nose gear model using a large aperture microphone directional array are reported in [16]. Unsteady pressure and acoustic measurements show that the torque arm section of the model exhibits the highest *rms* pressures and is also prominent in noise source maps. The far field acoustics scaled with the 6th power of flow speed and did not exhibit classical Strouhal scaling behavior.

B. The Plasma Fairing

It is well documented that a faired landing gear generates considerably less noise than the corresponding

unmodified gear. However, the need to access the gear for maintenance and stow the gear in cruise makes passive separation control via mechanical fairings impractical. Instead, dielectric barrier discharge (DBD) plasma actuators can be used for on-demand streamlining by creating a virtual "plasma fairing" that effectively streamlines gear components by active means The viability of achieving active noise control using dielectric barrier discharge (DBD) plasma actuators has been demonstrated through a series of complementary archival experiments and high fidelity numerical simulations. A prime motivation for the work is the recognition that airframe noise sources originate from a region of unsteady separated flow, which subsequently interacts with an airframe component. Any flow control strategy capable of minimizing or eliminating unsteady flow separation will prove beneficial in controlling airframe noise at the source. Numerous studies as reviewed in [17, 18] have demonstrated that DBD plasma actuators are ideally suited to separation control for a wide variety of practical aerodynamic applications. The basic characteristics of DBD plasma actuators are described in [19,20,21].

1. Single Cylinder Plasma Flow Control

The single cylinder is viewed as a generically relevant component flow geometry that is similar in all essential aspects to a landing gear oleo or strut. Effective flow control applied to a circular cylinder in cross-flow was the subject of a series of experiments and LES performed at Notre Dame as reported in a series of papers [22-25]. Two forms of plasma flow control were utilized. The first involved spanwise-oriented plasma actuators located on the cylinder surface just upstream of the separation location. These were found to be very effective at suppressing unsteady vortex shedding from the cylinder at high subcritical Reynolds numbers, $O(10^5)$. This resulted in substantial reduction of near-field pressure fluctuations in a frequency band centered on the Karman frequency. The spanwise plasma actuators could be operated in either steady or unsteady mode. In steady mode, control is achieved through near-wall momentum injection. LES and experiments showed that unsteady actuation at Strouhal numbers in the range $1 \leq St_D \leq 1.5$ was effective at totally suppressing Karman shedding. In the unsteady actuation case, the control is achieved by modification of the detached free shear layer. An alternate plasma flow control approach utilized a spnwise array of surface mounted actuators with electrodes oriented in the streamwise direction. These are employed in order to form plasma-induced streamwise vortices and this arrangement is called a "plasma streamwise vortex generator" (PSVG) [26]. Surface mounted PSVGs introduce streamwise vorticity into the nascent cylinder wake, which has the effect of promoting rapid wake mixing and there was a consequent elimination of Karman shedding.

*2. Tandem Cylinder Plasma Flow Control*

In landing gear, the flow over the undercarriage undergoes bluff body separation, is inherently unsteady, and is characterized by multiple wakes that interact with downstream gear components, thereby providing sources of broadband noise. Similarly, the tandem cylinder in cross-flow is a canonical bluff-body flow geometry that reproduces many of the essential aspects of the landing gear noise generation process. Of particular interest is the nature of the interaction of the unsteady wake from the upstream cylinder with the downstream cylinder and how it can be controlled.

Using either spanwise-oriented plasma actuators or PSVGs on the upstream cylinder, tandem cylinder flow control experiments and LES were performed over the Reynolds number range $22,000 \leq Re_D \leq 175,000$ as reported in [27,28]. Both methods of plasma flow control were shown to dramatically reduce surface pressure fluctuations on the downstream cylinder. As an example, Figure 1 compares two flow visualization images of the tandem cylinder configuration obtained at $Re_D = 22,000$ both without and with plasma flow control using the twin spanwise oriented actuators. Without plasma flow control, subcritical flow separation from the upstream cylinder occurs and gives rise to large-scale Karman vortex shedding. The near-wake subsequently impinges on the downstream cylinder in an unsteady manner. With plasma flow control, flow separation on the upstream cylinder is delayed and Karman
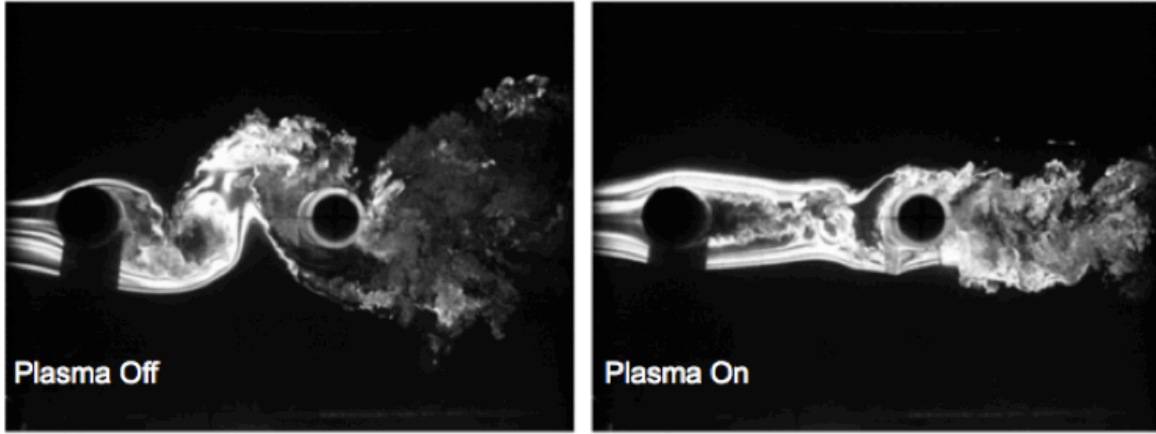
Figure 1. Tandem cylinder flow visualization with and without spanwise plasma actuation (from Kozlov and Thomas [28]).

shedding is obviously suppressed. The upstream cylinder wake is much thinner and its interaction with the downstream cylinder appears more dynamically benign than in the natural case. This was confirmed upon examination of the azimuthal variation in *rms* unsteady pressure fluctuations on the downstream cylinder. Figure 2 presents the *rms* pressure distribution, Cp_{rms}, both with and without plasma actuation. For the non-actuated case, peaks in Cp_{rms} are apparent. The largest, near 40° and 310°, correspond to the unsteady impingement of the wake from the upstream cylinder. The smaller peaks near 98° and 262° correspond to unsteady separation from the downstream cylinder. Figure 2 shows that the application of plasma actuation has a profound effect in reducing unsteady pressure fluctuations on the downstream cylinder. For example, the Cp_{rms} peaks near 40 and 310° are reduced by approximately 65%. Similarly, the Cp_{rms} peaks near 98° and 262° are reduced by 47%.
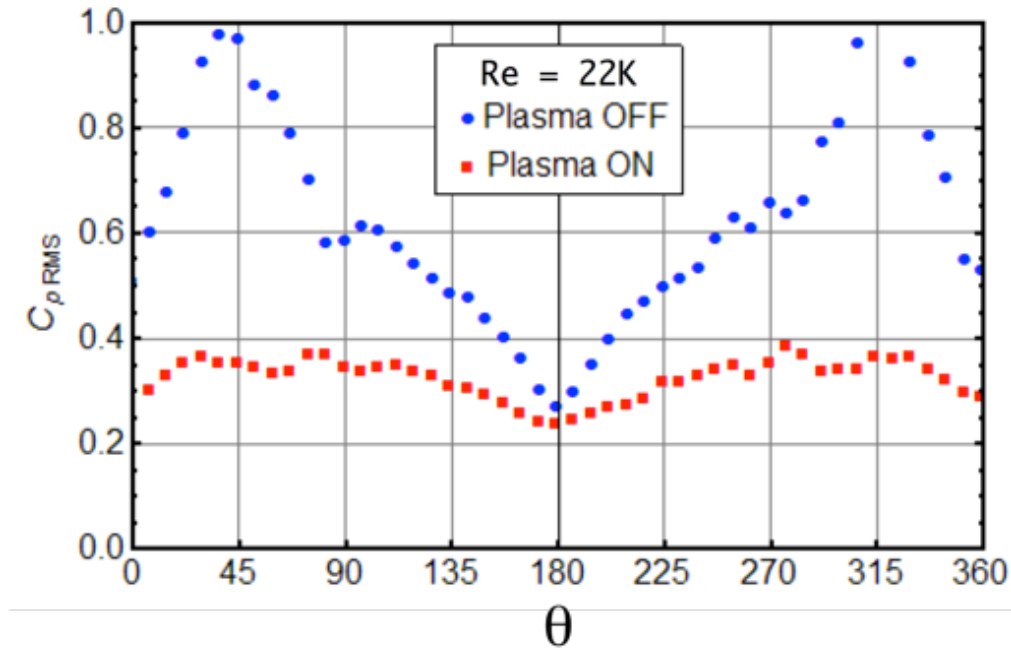
Figure 2. The effect of spanwise plasma actuation on the *rms* pressure distribution on the downstream cylinder (from [28]) .

The acoustic benefit of reducing wake-induced fluctuating surface pressure on radiated acoustics was recently demonstrated in [29]. The numerical approach utilized was based on LES for the turbulent flow field, a semi-empirical plasma actuation model, and Lighthill's theory for acoustic calculation. Excellent agreement between LES and the experimental results reported in [28] was obtained for both the baseline flow and flow with plasma control in terms of wake velocity profiles, turbulence intensity, and frequency spectra of pressure fluctuations on the downstream cylinder. The effectiveness of plasma actuators for reducing noise was clearly demonstrated. At a free-stream Mach number of 0.2, the peak sound pressure level is reduced by approximately 16 dB. This certainly confirms the viability of plasma actuation for active aeroacoustic control of airframe noise.

II. Motivation

In a first effort to extend the bluff-body plasma flow control technology demonstrated in the previous sections to a more realistic landing gear geometry, experiments and numerical simulations are presented in this paper which focus on the plasma flow control of the interaction between the hydraulic strut and torque arm of the G550 nose gear. This component work is considered prerequisite to the broader goal of demonstrating plasma noise control on a partially dressed, closed cavity 30% scale model of a Gulfstream G550 nose gear, which has been constructed at the University of Notre Dame.

III. Experimental Facility and Model

A model geometry simulating the aerodynamic interaction between the hydraulic strut and the downstream torque-arm components of the Gulfstream G550 nose gear was fabricated. The geometric motivation for the generalized tandem cylinder geometry is shown in Figure 3. This arrangement also forms a natural extension to the previous tandem cylinder plasma noise control studies reported by Kozlov and Thomas [28] and Eltaweel et al.[29].
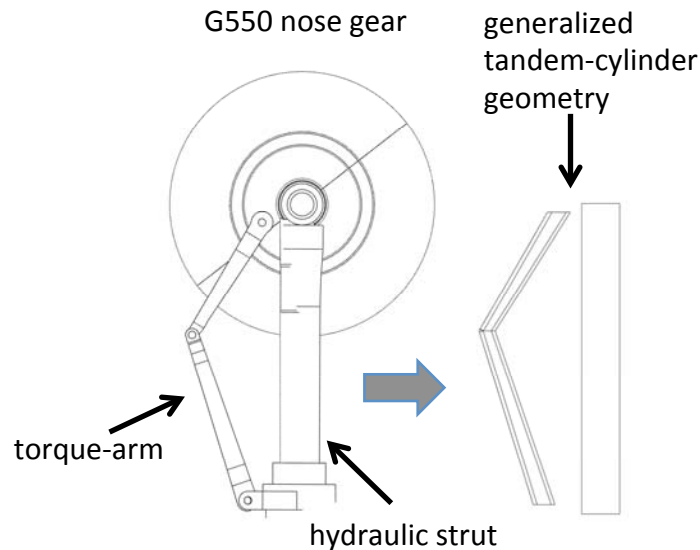
Figure 3. Comparison between the generalized tandem cylinder model and the G550 nose gear geometry.

As shown in Figure 3, a portion of the G550 landing gear is represented by a generalized tandem cylinder configuration. The two model components are shown schematically in more detail in Figure 4. The model consists of an upstream circular cylinder, which simulates the hydraulic strut with a simplified torque-arm model located downstream. The most notable modification of the torque arm from that on the G550 gear is the 0.635-cm-fillets added to each edge on the torque arm. These were added to reduce the high- frequency acoustic scattering content to allow a more exact comparison between experiment and computation at a reasonable computational cost.
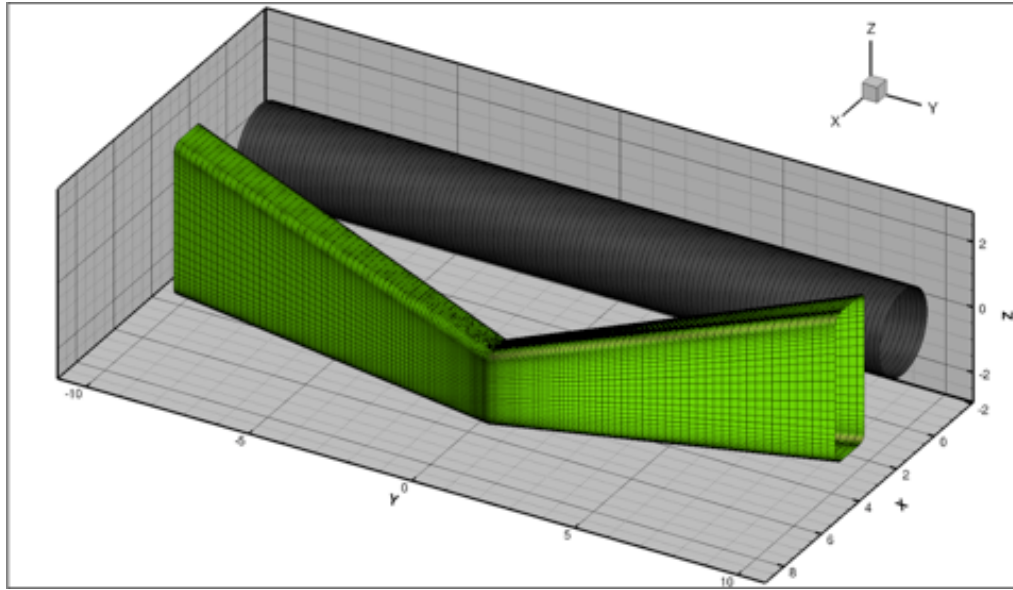
Figure 4: Simplified strut (circular cylinder) and torque arm configuration based on noise-critical regions of a Gulfstream G550 nose gear as reported in [16]. All dimensions are in inches.

The experiments were performed in one of the low-turbulence, subsonic, in-draft wind tunnels located at the Hessert Laboratory for Aerospace Research at the University of Notre Dame. The wind tunnel has an inlet contraction ratio of 20:1. A series of 12 turbulence management screens at the front of the inlet give rise to tunnel free stream turbulence levels less than 0.1% (0.06% for frequencies above 10 Hz). The maximum tunnel speed is approximately U_∞ = 35 m/s. Experiments are performed in a test section of 0.610 m square cross-section and 1.82 m in length.

The upstream cylinder model is equipped with two spanwise-oriented plasma actuators, as shown in Figure 5. The cylinder model is formed from a quartz glass cylinder with an outer diameter D = 65 mm, wall thickness d = 2.5 mm, a working span of 531.7 mm, and dielectric constant of 3.7. The cylinder wall serves as the dielectric barrier for the DBD plasma actuator. The ends of the cylinder terminate in plastic endplates, in order to minimize end effects.

As shown in Figure 5, the covered electrodes are common for both plasma actuators due to space limitations. As indicated, the outer, exposed electrodes (Figure 5, no. 2) are mounted to the surface of the cylinder with their plasma generating edges located at ±90° with respect to the approach flow direction. Both covered and exposed electrodes are made of Saint Gobain C661 1.6-mil (0.041- mm)-thick copper foil tape with acrylic adhesive. The foil thickness is very small compared with the local boundary-layer thickness so that the presence of the exposed electrodes did not change the subcritical flow separation from the cylidner. The thickness of the surface electrodes shown in Figure 5 is greatly exaggerated. The covered electrode (Figure 5, no. 3) is mounted to the inner surface of the cylinder. Both inner and outer electrodes extend 310 mm in span between model endplates. Eight layers of 5-mil (0.127-mm)-thick Kapton tape (Figure 5, no. 4) cover the inner electrodes and serve to prevent inner discharge. The inner and outer electrodes for the spanwise actuator have a small overlap, which gives rise to a large local electric field gradient. Plasma discharge (Figure 5, no. 5) forms near the edge of the exposed electrodes and extends a distance along the cylinder's dielectric surface over the convered electrode. As indicated in Figure 5, the actuators are connected to a high-voltage ac source. In this study, the spanwise actuators use a sine waveform ac voltage of 40 kV peak-to-peak at 2 kHz. The high voltage is measured with a LeCroy PPE20kV dc high-voltage probe in conjunction with a LeCroy LT262 oscilloscope. These ac voltage amplitudes were held constant for the entire Reynolds number range investigated in the flow control experiments. That is, all of the results reported here are attained without any effort to optimize the plasma actuator.

American Institute of Aeronautics and Astronautics
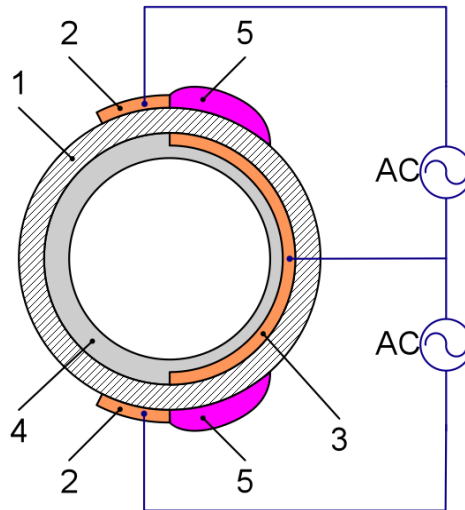
Figure 5. Plasma flow control applied to the upstream cylinder model. (1) quartz cylinder, (2) surface electrodes, (3) common covered electrode, (4) internal Kapton insulation, (5) plasma forming region.

Flow visualization experiments were performed using a TSI particle image velocimetry CAM 10-30 digital camera in conjunction with a Y120-15 New Wave Research Nd:Yag laser. Continuous DEHS fog consisting of nominally 1-mm-diameter droplets generated by a TSI six-jet particle atomizer were introduced upstream of the wind-tunnel inlet contraction. The Nd:Yag laser was used to illuminate the fog in spanwise planes consistent with the locations at which Endevco unsteady surface pressure sensors were mounted on the downstream torque arm model. Flow visualization was performed with both the plasma on and off in order to assess the global influence on the wake interaction with the torque arm.

The unsteady surface pressure was measured with flush surface-mounted Endevco model 8515C-15 miniature absolute piezoresistive pressure transducers with 15psi (103.4 kPa) pressure range. The pressure transducers have a diameter of 2.34 mm and were positioned at key locations on the torque-arm as shown in Figure 8. Each of these locations has been identified as a region of significant noise production. Location 2 is of particular interest as its coordinates correspond to the area of largest measured Cp_{rms} in Neuhart et al [15]. The surface pressure at each location was measured under both natural and plasma flow control conditions. The sensor signal was conditioned by amplifier (Endevco model 136) and acquired by a personal computer using a Microstar iDSC 1816 A/D board. This board has onboard fourth-order analog antialiasing filters. Measurements of the unsteady RMS surface pressure on the downstream torque arm were performed. Additionally, power spectra were calculated to reveal the frequency composition of the pressure fluctuations. The 95% relative uncertainty in measured Cp_{rms} is less than ±2.5%.

IV. Numerical Approach

The NPARC Alliance's Wind-US [30, 31, 32] Navier-Stokes solver was used to model the flow over the strut and torque arm assembly shown in Figure 4 which was also tested in the Notre Dame wind tunnel. Wind-US is a broadly capable production code which has a number of different numerical methods implemented within it [33,34,35]. Wind-US supports both implicit and explicit time integration. For unsteady runs where larger time steps are required than the explicit Runge-Kutta schemes will permit, a second order implicit scheme is available, and Newton subiterations or dual timestepping can be used to further improve temporal accuracy. Both abutting and overlapped zone-to-zone coupling modes are supported, as is structured-to-unstructured zonal coupling.

ITAC has extensive experience developing and using this solver for a variety of applications, including steady-state Reynolds-averaged Navier-Stokes cases [36,37] and time-accurate simulations [38,39]. While Wind-US is not a computational aeroacoustics solver, *per se*, it has a number of numerical methods available which allow it to successfully compute a wide variety of unsteady flows. For the current work, we made use of a hybrid spatial scheme which blends a 2nd order central method (80% weighting) with a 3rd order upwind-biased scheme (20% weighting). The resulting scheme is fairly stable without having the overwhelming numerical dissipation which conventional RANS methods often have. To ensure accurate time marching, a second order implicit scheme was employed in conjunction with a dual time stepping method (12 subiterations per time step).

An ILES variant of the Spalart DES model [40] for turbulence was used for this work. In the conventional DES approach, the model switches from a RANS model (Spalart-Allmaras) near solid boundaries to a Smagorinsky-like LES model away from them. In the ILES variant, the explicit turbulence model turns itself completely off away from solid boundaries, and the simulation instead relies on the inherent numerical dissipation of the solver to ensure a reasonable cascade of resolved turbulent energy into the unresolved subgrid scales.

Key to the numerical simulations discussed here has been ITAC's access to the Notre Dame plasma model utility. This code was provided to ITAC and was reimplemented by ITAC as stand-alone utility. We were thus able to configure this solver to compute the average body force due to one of the two actuators on the circular cylinder. This 2-D field was saved to a file which is then read by the Wind-US solver. The user specifies the location, orientation and extend (in the third dimension) of the region where the body force is to be applied. The force magnitude can also be manipulated. A preliminary capability that allowed use of the plasma actuator body force was implemented and used in Wind-US for a previous ITAC project. That capability was significantly upgraded and generalized for the current work in order to allow the plasma actuators to be modeled on the curved cylinder surface with its attendant curvilinear computational mesh.

The computational domain extent, along with the strut and torque arm model is shown below in Figure 6. The basic mesh topology consists of body-fitted curvilinear meshes in the near-body region around the strut and torque arm, and then stretched Cartesian meshes in the remainder of the domain. Based on the lessons learned from earlier computational efforts, the current mesh has been designed such that the overlapping regions where the near-body meshes interact with the Cartesian meshes have approximately equivalent mesh resolution (see Figure 7). Also shown in this plot is the region of increased grid density between the strut and the torque arm, which is designed to better resolve the unsteady flow structures which are shed from the former and impact the latter (and are believed responsible for much of the noise generation in this configuration). The resulting final mesh had roughly 55 million cells.
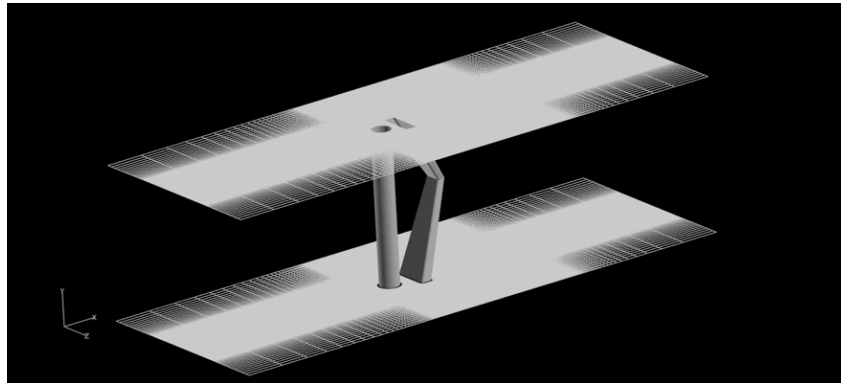

Figure 6: Computational domain extent
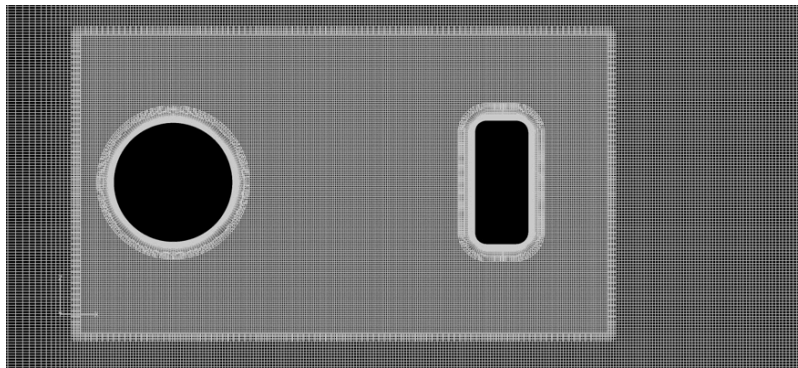
Figure 7: Y=0.0 cross-section of computational mesh in region about the strut and torque arm

Two cases were simulated for the current work. Both had the same geometric, flow conditions, and solver settings; they differed only in that one included the effect of plasma actuators and the other did not. The reference total pressure was 98,732 Pa. The total temperature was 286.8 K, and the tunnel velocity was 28 m/s. A time step of 6.67e-7 seconds was used throughout.

For the case with actuation, two plasma actuators were modeled as in the experiment, with the interfaces between the covered and exposed electrodes positioned at +/- 90 degrees on the leading cylinder relative to the oncoming flow. They were oriented in order to accelerate the flow downstream (via wall jets along the cylinder surface), and thereby delay separation.

While the numerical simulations saved pressure data on the entire torque arm surface for the entire run, the three pressure tap locations used in the tunnel were used for comparison with experiment. These locations are shown below in Figure 8. Of the three points, P2 corresponds to a location that has been found in previous work to be critical to noise generation on the G550 landing gear.
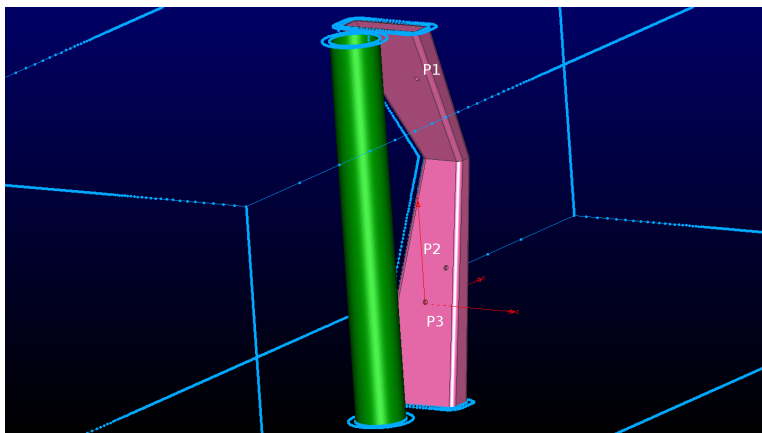
Figure 8: Locations of pressure taps in wind tunnel experiments

V. Numerical Results

The plasma off and plasma on cases were decomposed from the original seven blocks into 128 blocks to allow efficient parallel processing on ITAC's in-house compute cluster. The solutions were obtained using either 64 or 128 processors (depending on the system load at the time). The case with plasma actuation was run for a total of 10,682 time steps, while the baseline unactuated case ran for 22,345. The difference in the number of steps in the different solutions is due in part to the need for a longer run of the unactuated case in order to obtain reliable statistics. The actuated case was much more stable in this statistical sense, and therefore did not require as long of a run to obtain usable results.

A. Qualitative Analysis

The results of the simulations clearly show a strong impact of plasma actuation on the flow. For example, in Figure 9 below, it is apparent that the addition of actuation has greatly reduced the unsteady separation from the strut (on the particular cross-section shown). The result of this is that the flow downstream of the torque arm is behaving more as an isolated system for the actuated case, as compared to the more complex interactions seen in the baseline case. The strut wake interaction with the torque arm is reduced and the torque arm sheds vorticity more like and isolated body.

Similar behavior is seen in the plot of pressure gradient magnitude (on the same cross-section) shown below in Figure 10. The effects of the plasma-induced body force which has been applied in the actuated case can be seen in the vicinity of the strut in the actuated case. Note the fore-aft symmetry in the strut pressure field associated with the application of plasma flow control.

A more global view of the effects of plasma actuation can be seen in Figure 11. A general reduction in the extent of vortical structures is seen throughout the actuated case (Figure 11b), but is particularly notable in the
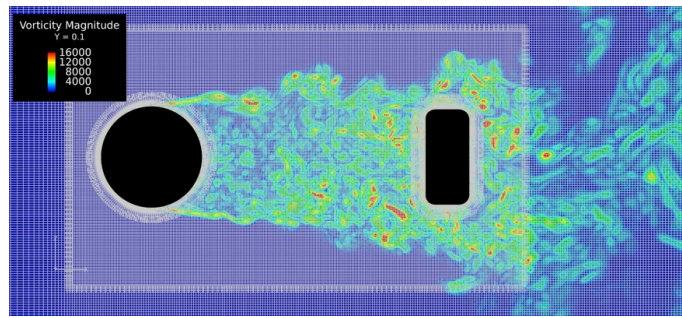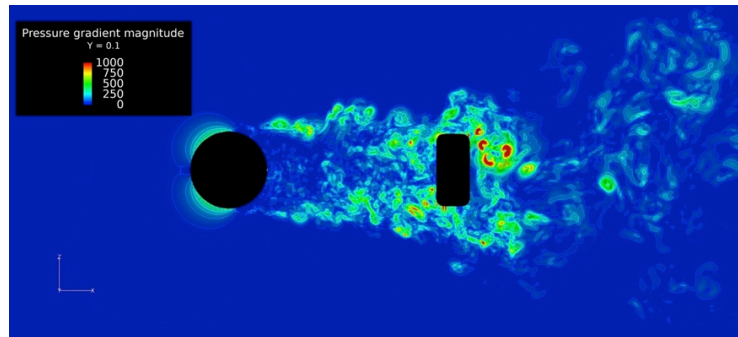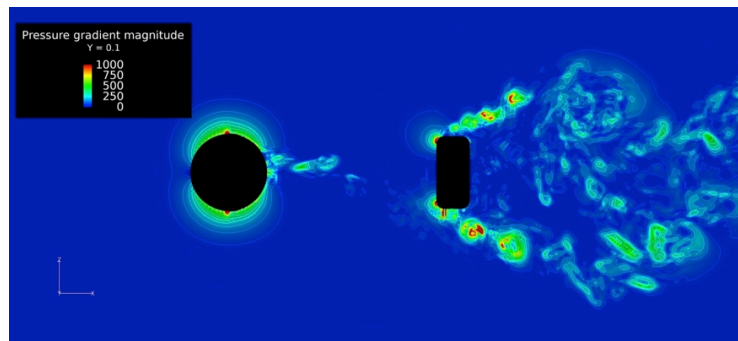
a) Baseline Case
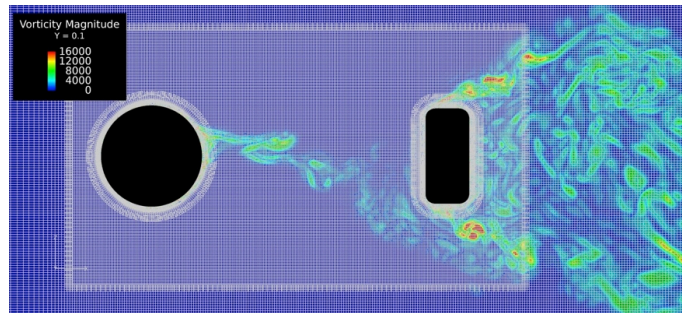
b) Actuated Case

Figure 9: Vorticity magnitude at a constant spanwise cross-section in the region between the strut and torque arm.
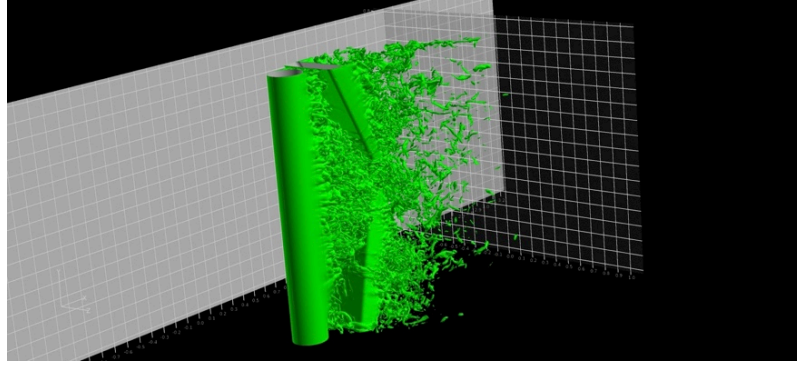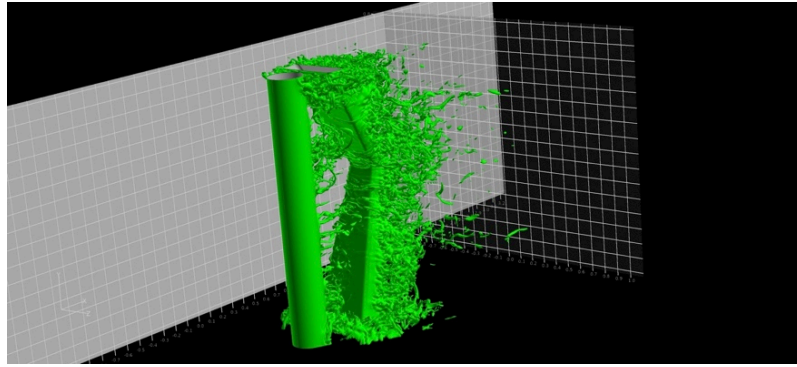

a) Baseline Case

b) Actuated Case

Figure 10: Pressure gradient magnitude on a constant spanwise plane for natural and actuated cases.

a) Baseline Case

b) Actuated Case

Figure 11: Iso-surface of vorticity (8000 level) in the baseline (a) and plasma actuated (b) flow fields.

region between the strut and torque arm. Note the increased vortical structures in the wake of the torque arm suggesting that shedding from the torque arm has become more independent of the upstream strut.

B. Quantitative Analysis

To obtain a more quantitative assessment of the results, we examined the predicted pressure coefficient of the unsteady pressure Cp_{rms} at each of the locations for both actuated and unactuated cases

$$Cp_{rms} = \frac{(p-p_{ref})_{rms}}{0.5\rho_{ref}V_{ref}^2}$$

(1)

There was some concern as we performed our initial analysis that we had not achieved a statistically stationary signal and also that there might be interference in our simulations from pressure waves bouncing back and forth between the upstream and downstream boundaries (despite the damping introduced near the boundaries to prevent this). Thus, a further analysis was performed which attempted to filter out any such possible contamination.

The first step in this process was to perform a digital Fourier transform of the portion of the pressure signals which we previously used for predicting the earlier estimates of Cp_{rms}. Such a transform, however, will be contaminated by the fact that the pressure traces are not actually perfectly periodic. This introduces errors in the resulting spectrum. This is often dealt with through the use of a windowing function, such as that of Hanning or Hamming. For the current work, we have taken a slightly different approach.

The elements of the initial spectrum were multiplied by the corresponding wavenumber and the maximum of this quantity was identified. The wavenumber where this maximum occurs represents the frequency which has the strongest impact on the signal. The period corresponding to this wavenumber is next identified, and a linear "splice" with a length of half the period is created which connects the value at the beginning of the signal to the value at the

end of the signal. The result is a signal which is periodic, but the modification has been done so as to minimize the errors due to the non-periodicity of the original data.

To explore the possible impact of signal contamination at the lowest frequencies, a high-pass filter was implemented which allows the user to specify a wavenumber below which the contributions are progressively damped using a cosine function

$$FAC = 0.5 - 0.5\cos(\pi k/k_{cut}), \ k \leq k_{cut} \tag{2}$$

Thus, for a cutoff wavenumber of 4, for example, this function will almost completely eliminate the first wavenumber, strongly damp the second, and somewhat reduce the contribution of the third wavenumber. The fourth wavenumber's contribution is unchanged. The intention of this procedure is to reduce or eliminate the impact of one-time events and, in general, the influence of wavenumbers for which only a few samples are present in the time history (and therefore are not statistically stationary).

Results for Cp_{rms} were obtained for the simulated pressure histories for the unfiltered data, and with cutoff wavenumbers of 4 and 8 and these are compared in Table 1.

Table 1. Cp_{rms} Computed with Different High-Pass Filter Cut-off Wavenumbers

Cut –off k	P1 (baseline)	P1 (plasma)	P2 (baseline)	P2 (plasma)	P3 (baseline)	P3 (plasma)
0	0.4163	0.1829	0.3485	0.1641	0.2616	0.1382
4	0.3519	0.1471	0.3379	0.1523	0.2485	0.1126
8	0.2704	0.1211	0.3272	0.1428	0.2316	0.0953

From the results in Table 1, it is clear that the data at locations P2 and P3 are relatively statistically stationary. This is apparent because, as the cut-off frequency is increased, the predicted Cp_{rms} changes only a small amount. At Point 1, however, significant changes are seen as the cut-off wavenumber changes. This indicates that the larger scales, for which only a few samples are present in the time series, are playing a large role in determining the value of Cp_{rms} at this locations. Given the expected range of scales in this flow, it is likely that the result at location P1 for a cut-off wavenumber of 8 is the best estimate for the unsteady pressure coefficient which would be obtained if the simulation were continued far enough to achieve a true stationary result. Interestingly, the most consistent results are obtained at location P2, which has been shown to be one of the most critical, in terms of importance for noise generation.

Using the cut-off wavenumber of 8 values, the simulation predicts a plasma flow control induced reduction in Cp_{rms} of 55%, 56.4% and 59% at locations P1, P2 and P3, respectively. The Cp_{rms} values in Table 1 will be compared with experimental values of Cp_{rms} presented in the following section.

VI. Experimental Results

In this section results from experiments performed at the University of Notre Dame wind tunnel facility are presented. These include qualitative flow visualization that document the global effect of the plasma flow control on the strut-torque arm configuration, followed by quantitative measurements of unsteady surface pressure at selected locations.
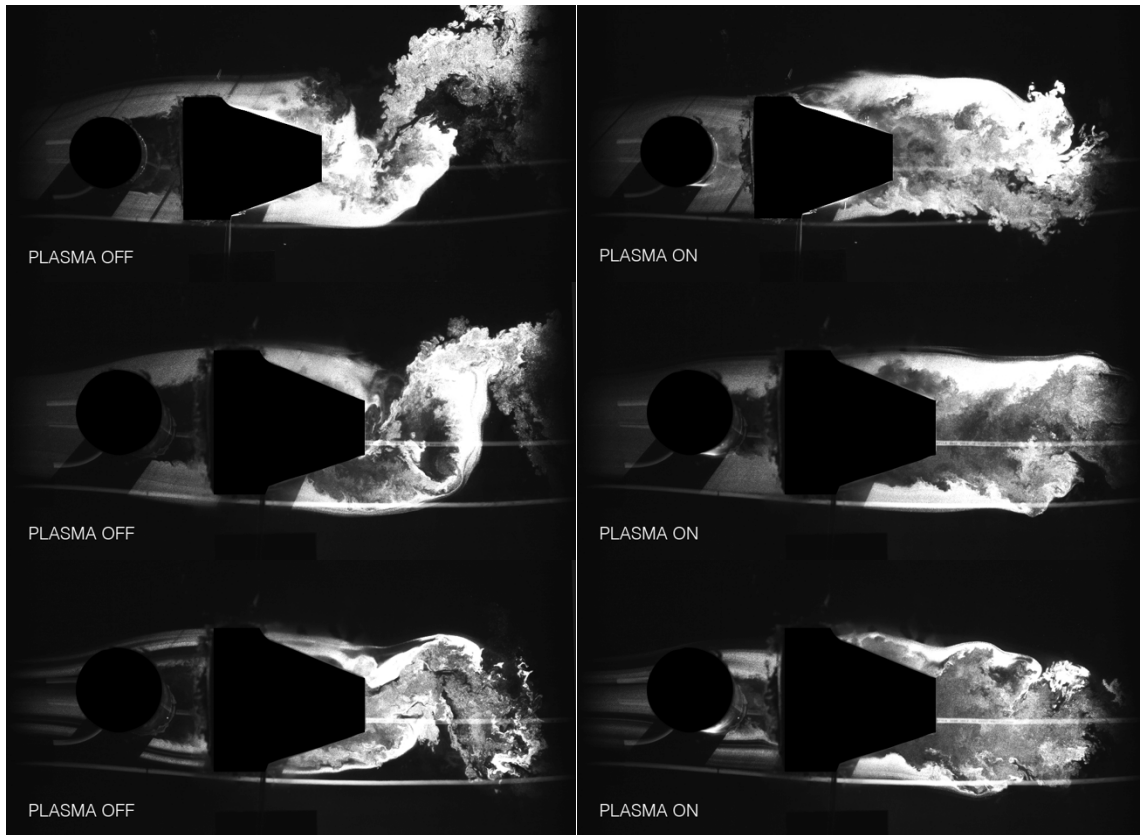
A.   Flow Visualization Results
Zdravkovich [41] comprehensively reviewed flow around two circular cylinders of the same diameter in a tandem configuration at subcritical Reynolds number and described key flow regimes. These classifications are based mainly on the parameter *L/D* where *L* is the center-to-center distance between the front and rear cylinders, and *D* is the cylinder diameter. Although the geometry considered here is more complex, these criteria still provide some guidance with regard to the anticipated character of the flow. Due to spanwise asymmetry of the rear torque arm the surface pressure sensor locations were selected to explore two key regimes outlined by Zdravkovich: Location P1 is at an L/D $\approx$ 1.5 which is expected to be associated with the formation of a separation bubble behind the upsteam cylinder (strut) with vortex shedding occurring primarily from the torque arm. Locations P2 and P3 correspond to *L/D* = 1.94 and 1.9, respectively, and are expected to be associated with quasi-steady reattachment of shear layers from the upstream cylinder on the downstream torque arm. Of course, the cylinder-torque arm spacing varies in the

spanwise direction so the flow behavior may well encompass mode switching behavior as well.

Representative flow visualization images of the baseline and plasma actuated flows obtained in spanwise planes corresponding to locations P1, P2 and P3 (for reference see Figure 8) are presented in Figure 13. To obtain the best flow visualization, these images were acquired at a comparatively modest $Re_D = 58,000$. Note that the natural flowfield at all three-measurement planes seems to behave as a single body due to the small separation between the strut and torque arm. Shear layers undego subcritical separation from the front cylinder (strut) and subsequently give rise to an unsteady interaction with the edges of the torque arm. The shear layer interaction gives rise to very large-scale von Karman vortex shedding downstream of the torque arm.

With plasma flow control applied, flow visualization shows that the separation on the cylinder is obviously delayed (due to tangential momentum injection), giving rise to a quasi-steady strut wake interaction with the downstream torque arm. In fact, the P1 image shown in Figure 13 bears a strong resemblance to the plasma actuated tandem cylinder image shown previously in Figure 1. As a consequence of the flow control, the wake downstream of the torque arm is charactrerize by smaller scale apparently symmetric vortex shedding and the large-scale von Karman shedding obsetved in the baseline case is absent. Figure 13 shows similar results for the plasma actuated cases shown in planes P2 and P3.


Figure 13. Flow visualization of the baseline (left) and plasma actuated flow (right) at Re = 58,000 in plane P1 (top), P2 (middle), and P3 (bottom).

B. Fluctuating Surface Pressure Specta

Surface pressure fluctuations were measured at sensor locations P1, P2 and P3 (see Figure 8) for $Re_D = 122,000$ corresponding to $M = 0.081$. Figure 14 compares the measured values of Cp_{rms} for both the baseline and plasma actuated cases. As indicated the plasma actuation reduces Cp_{rms} at locations P2 and P3 but has little effect at location P1. Reductions of 13% and 7% occur at locations P2 and P3, respectively.

Comparison with the CFD results shown previously in Table 1 reveals that the impact of actuation is clearly over-estimated in the simulations compared to the experimental findings. The most obvious candidate to explain this is that the volumetric body force which is being used to model the effect of the plasma actuators has been
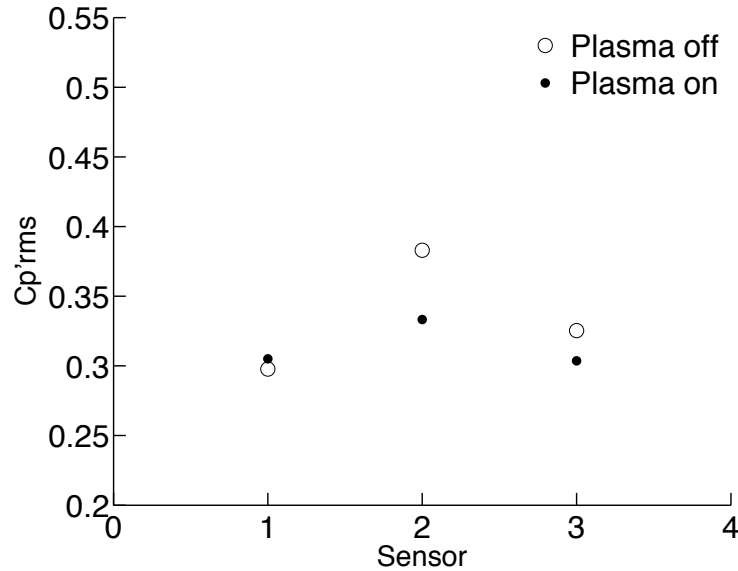
Figure 14. Effect of plasma actuation on *rms* fluctuating surface pressure coefficient at each sensor location for Re = 122,000

improperly implemented in the Wind-US solver, and it is therefore necessary to check the values in the field and the code itself to ensure that an improper scaling factor (or other error) has not been introduced.

Figure 15 presents corresponding measurements of power spectral density (PSD) corresponding to these three locations for both baseline and plasma control cases. The power spectral density in dB (referenced to 20 μPa) is plotted as a function of Strouhal number ($St = f D / U$).

For location P1, plasma flow control is shown to have a slight detrimental effect. In contrast, for position P2, which was shown in the study of Neuhart et al [15] to correspond to the highest level pressure fluctutations, the plasma flow control has a very significant effect in reducing the spectral content near $St_D = 0.17$ which is associated with vortex shedding from the upstream cylinder. The spectral peak is reduced by approximately 5 dB. Similar behavior is noted in the spectra shown at location P3. A broad spectral peak at $St_D = 0.17$ is reduced by 3 dB. While the effect of plasma actuation is not as drastic as at P2, this might be expected because the sensor at P3 is located at the centerline of the torque arm.

It is also instructive to examine the surface pressure spectra in pre-multiplied form. An example is shown in Figure 16 which presents baseline and plasma actuated surface pressure spectra obtained at location P2 in scaled form. For the baseline case a sharp peak is shown near $St_D = 0.17$ and this is associated with unsteady vortex shedding from the upstream cylinder. When plasma is applied, this spectral peak is greatly reduced in amplitude. This demonstrates the effectiveness of the plasma flow control at eliminating Karman shedding from the upstream cylinder. Note however, that the plasma flow control actually *increases* the spectral content at higher St_D with a peak near $St_D = 0.4$. This high frequency content will obviously lesson the effect of the plasma flow control in reducing Cp_{rms}. Behavior similar to this was reported in the tandem cylinder plasma flow control study by Eltaweel et al [29]. Their results showed that a reduced spectral peak near $St_D = 0.2$ for the actuated case was actually due to shedding from the downstream cylinder, while a new peak at $St_D = 0.4$ was found associated with shedding from the upstream cylinder. The higher Strouhal number was a consequence of a reduced characteristic length scale for separation due to the plasma flow control. It is suspected that a similar mechanism may be in play here. This aspect will need to be further explored in order to achieve maximum reduction in overall Cp_{rms}.

Despite the disparity in the experimental results and the simulated effect of actuation, both are in agreement in the sense that plasma actuation is shown to act to reduce the unsteady pressure coefficient at critical points on the torque arm. This, in turn, has been shown to reduce the resulting noise emitted by such configurations. This possibility is the subject of our ongoing research.
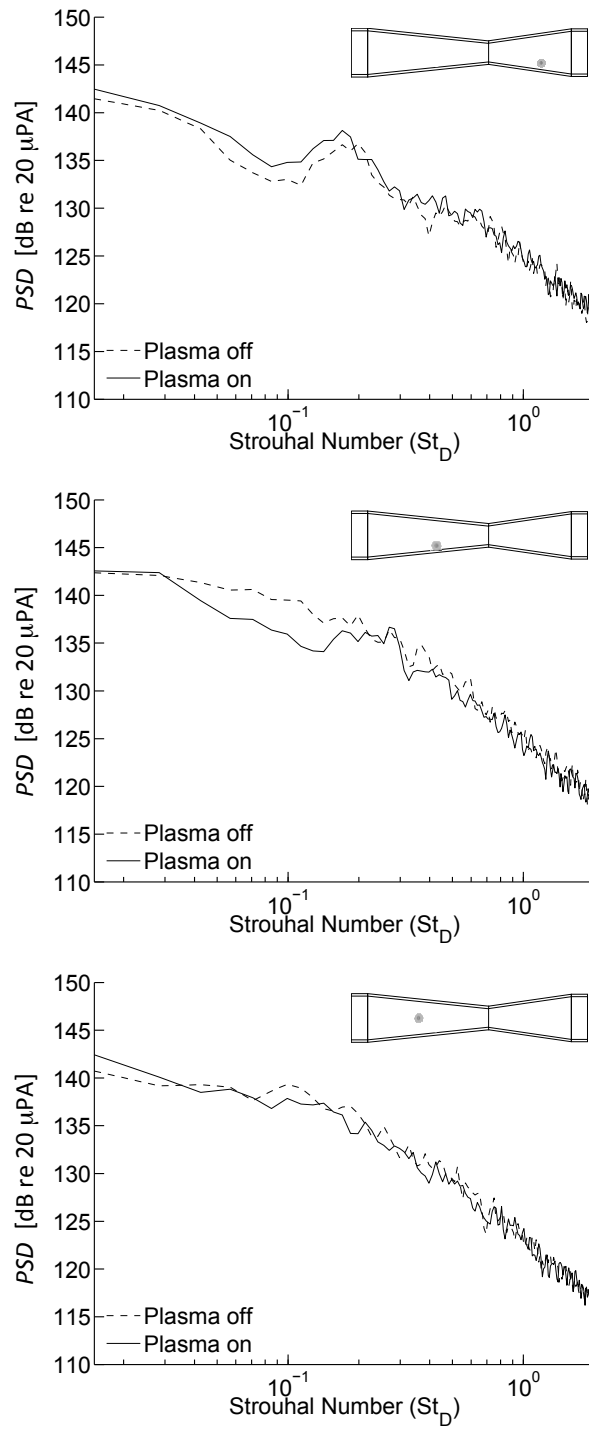
Figure 15. Torque arm fluctuating surface pressure power spectra density (with reference to 20e-6 Pa) Sensor location P1 (top), P2 (middle), and P3 (bottom) for Re = 122,000.

American Institute of Aeronautics and Astronautics
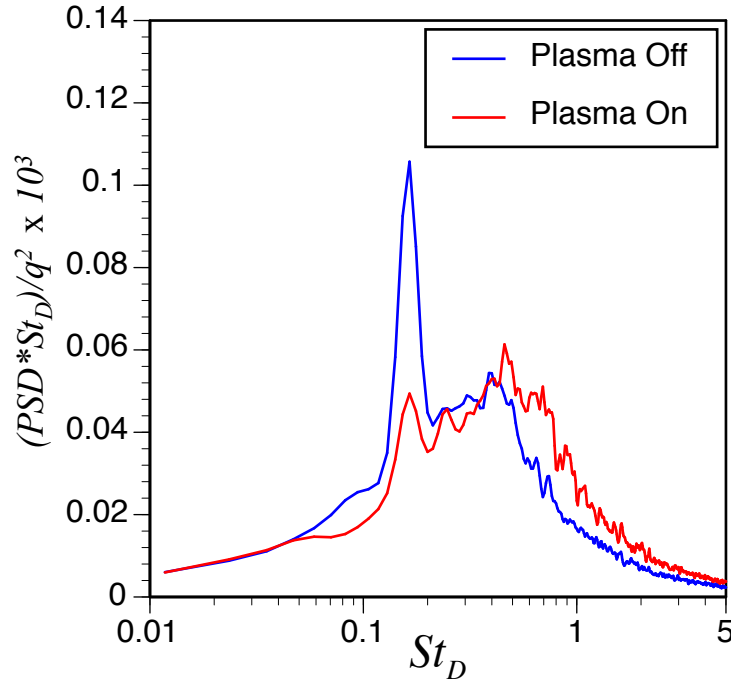
Figure 16. Pre-multiplied surface pressuer fluctuation spectrum at location P2 for baseline and plasma cases. Re$_D$ = 122,000.

VII. Conclusion

The flow control experiments presented in this study demonstrate that DBD plasma flow control in the form of twin spanwise-oriented actuators located on the upstream strut, is effective at reducing the *rms* surface pressure fluctuations on the downstream torque arm. Both experiments and numerical simulations show that large-scale vortex shedding from the upstream cylinder is suppressed by twin plasma-induced wall jets that delay flow separation from the upstream cylinder. With plasma flow control the resulting wake interaction with the downstream torque arm is quasi-steady.   The degree of pressure fluctuation suppression depends on the position on the torque arm. As one may expect, the benefit appears greatest for locations near the edges which are associated with shear layer impingement from the upstream strut. The numerical simulations predict larger reductions in Cp_{rms} than are realized in the experiments suggesting the need to re-evaluate the implementation of the plasma-induced body force in the simulation. The experiments show that although the plasma reduces pressure fluctuations associated with vortex shedding, at certain locations it actually increases high frequency content and this effect needs further exploration since this limits the reduction in Cp_{rms}. Further reduction in unsteady surface pressure on the downstream torque arm should be possible by optimizing the electrode azimuthal placement, plasma frequency, and applied voltage. This is considered prerequisite to the goal of full plasma fairing control of the G550 noise gear for noise reduction.

References

[1] Lockard, D. P. and Lilley, G. F., "The Airframe Noise Challenge," NASA/TM- 2004-213013, 2004.

[2] Michel, U., Barsikow, B., Helbig, J., Hellmig, M., and Schuttpelz, M., "Flyover Noise Measurements on Landing Aircraft with a Microphone Array," AIAA paper 1998-2336, 1998.

[3] Lazos, B., "Surface Topology on the Wheels of a Generic Four Wheel Landing Gear," *AIAA J.*, 40, 12, pp. 2402-2411, 2002.

[4] Li, F., Khorrami, M. R., and Malik, M. R., "Unsteady Simulation of a Landing- Gear Flow Field," AIAA paper 2002-2411, 2002.

[5] Lockard, D. P., Khorrami, M. R., and Li, F., "Aeroacoustic Analysis of a Simplified Landing Gear," AIAA paper 2003-3111. 2003.

[6] Jenkins, L. N., Khorrami, M. R., Choudhari, M. M., McGinley, C. B., "Characterization of Unsteady Flow Structures Around Tandem Cylinders for Component Interaction Studies of Airframe Noise," AIAA paper 2005-2812, *11th AIAA/CEAS Aeroacoustics Conference*, 2005.

[7] Jenkins, L.N., Neuhart, D.H., McGinley, C. B., Choudhari, M. M., Khorrami, M. R., "Measurements of Unsteady Wake Interference Between Tandem Cylinders," AIAA paper 2006-3202, 2006.

[8] Khorrami, M. R., Choudhari, M. M., Jenkins, L. N., McGinley, C. B., "Unsteady Flowfield Around Tandem Cylinders as Prototype for Component Interaction Airframe Noise," AIAA paper 2005-2866, *11th AIAA/CEAS Aeroacoustics Conference*, May 2005, Monterey, CA.

[9] Neuhart, D. H., Jenkins, L. N., Choudhari, M. M., Khorrami, M., "Measurements of the Flowfield Interaction Between Tandem Cylinders," AIAA paper 2009- 3275, *15th AIAA/CEAS Aeroacoustics Conference*, May 2009, Miami, FL.

[10] Hutcheson, F., and Brooks, T., "Noise Radiation from Single and Multiple Rod Configurations," AIAA paper 2006-2629.

[11] Dobrynski, W., Pott-Pollenske, M., Foot, D. and Goodwin, M., "Landing Gears Aerodynamic Interaction Noise," Proceedings of the European Congress on Computational Methods in Applied Sciences and Engineering, P. Neittaanmäki, T. Rossi, S. Korotov, E. Oñate, J. Périaux, and D. Knörzer (eds.), Jyväskylä, 24- 28 July 2004.

[12] Remillieux, M. C., "Aeroacoustic Study of a Model Landing Gear in a Semi- Anechoic Wind Tunnel," M. S. Thesis, Virginia Polytechnic Institute and State University, Blacksburg, VA, 2003.

[13] Horne, C., James, K. D., Arledge, T. K., Soderman, P. T., Burnside, N., Jaeger, S.M., "Measurements of 26%-scale 777 Airframe Noise in the NASA Ames 40 X 80 Foot Wind Tunnel," AIAA paper 2005-2810, *11th AIAA/CEAS Aeroacoustics Conference*, 2005.

[14] Rackl, R. G., Miller, G., Guo, Y., Yamamoto, K., "Airframe Noise Studies- Review and Future Direction," NASA/CR-2005-213767, 2005.

[15] Neuhart, D. H., Khorrami, M. R. and Choudhari, M. M., "Aerodynamics of a Gulfstream G550 Nose Landing Gear Model," AIAA Paper 2009-3152, 15th AIAA/CEAS Aeroacoustics Conference, Miami, FL, 2009.

[16] Zawodny, N. S., Liu, F., Yardibi, T., Cattafesta, L., Khorrami, M. R., Neuhart, D. H., Van de Ven, T., "A Comparative Study of a 1⁄4 -Scale Gulfstream G550 Aircraft Nose Gear Model," AIAA Paper 2009-3153, 15th AIAA/CEAS Aeroacoustics Conference, Miami, FL, 2009.

[17] Corke, T. C., Post, M. L., Orlov, D. M., "Single Dielectric Barrier Discharge Plasma Enhanced Aerodynamics: Physics, Modeling and Application," Exp. Fluids, 46, 2009, pp. 1-26.

[18] Moreau, E., "Airflow Control by Non-Thermal Plasma Actuators," *J. Phys D Appl Physics*, 40, pp. 605-636.

[19] Fridman, A., and Kennedy, L. A., *Plasma Physics and Engineering*, Taylor & Francis, New York, 2004.

[20] Enloe, C. L., McLaughlin, T. E., VanDyken, R. D., Kachner, K.D., Jumper, E. J., Corke, T. C., Post, M., and Haddad, O., "Mechanisms and Responses of a Single Dielectric Barrier Plasma Actuator: Geometric Effects," AIAA Journal, 42, 3, 2004, pp. 595-604.

[21] Enloe, C. L., McLaughlin, T. E., VanDyken, R. D., Kachner, K.D., Jumper, E. J., Corke, "Mechanisms and Responses of a Single Dielectric Barrier Plasma Actuator: Plasma Morphology," AIAA Journal, 42, 3, 2004, pp. 589-594.

[22] Thomas, F. O., Kozlov, A., and Corke, T. C., "Plasma Actuators for Cylinder Flow Control and Noise Reduction," *AIAA Journal*, Vol.46, No.8, pp 1921-1931, 2008.

[23] Kozlov, A. and Thomas, F. O., "Active Control of Bluff Body Flows Using Dielectric Barrier Discharge Plasma Actuators," AIAA-2009-3245, 15th *AIAA/CEAS Aeroacoustics Conference*, Miami, FL, 2009.

[24] Kozlov, A. V., and Thomas, F. O., "Control of Bluff Body Flow Via Two Types of Dielectric Barrier Discharge Plasma Actuation," *AIAA Journal*, in review, 2010.

[25] Kim, D., and Wang, M.,"Large Eddy Simulation of Flow Over a Circular Cylinder with Plasma Based Control," AIAA Paper 2009-1080, 47th AIAA Aerosapce Sciences Meeting, Orlando, FL, 2009.

[26] Wicks, M., Thomas, F. O., Schatzman, D., Bowles, P., Corke, T. C., Patel, M., Cain, A., "A Parametric Investigation of Plasma Streamwise Vortex Generator Performance," AIAA paper 2012-0824, presented at the 50th Aerospace Sciences Meeting, Nashville, TN, 2012.

[27] Thomas, F. O., Kozlov, A. V., ELTaweel, A., Wang, M. and Kim, D."Plasma Flow Control of Cylinders in a Tandem Configuration: Experiment and Large Eddy Simulation," AIAA Paper 2010-3790, 16th AIAA/CEAS Aeroacoustics Conference, Stockholm, Sweden, 2010.

[28] Kozlov, A. V., and Thomas, F. O., "Plasma Flow Control of Cylinders in a Tandem Configuration," *AIAA Journal*, Vol. 47, No. 10, pp. 2183-2193, 2011.

[29] Eltaweel, A., Wang, M., Kim, D., Thomas, F. O., Kozlov, A., "Numerical Investigation of Tandem-Cylinder Noise Reduction using Plasma-Based Flow Control," *J. Fluid Mech.*, Vol. 756, pp. 422-451, 2014.

[30] Bush, R. H., Power, G. D., and Towne, C. E., 1998, "WIND: The Production Flow Solver of the NPARC Alliance," AIAA Paper 98-0935.

[31] Power, G. D. and Underwood, M. L., 1999, "Wind 2.0- Progress on an Applications-Oriented CFD Code," AIAA Paper 99-3212.

[32] Nelson, C. C. and Power, G. D., 2001, "CHSSI Project CFD-7: The NPARC Alliance Flow Simulation System," AIAA Paper 2001-0594.

[33] Nelson, C. C., Lankford, D. W., and Nichols, R. H., 2004, "Recent Improvements to the Wind-(US) Code at AEDC," AIAA Paper 2004-0527.

[34]Mani, M., Cary, A., Ramakrishnan, S. V., 2005, "A Structured and Hybrid-Unstructured Grid Euler and Navier-Stokes Solver for General Geometry," *Journal of Aircraft*, Vol 42, No 4.

[35]Georgiadis, N. J. Yoder, D. A., Towne, C. E., Engblom, W. A., Bhagwandin, V., Lankford, D. W., Power, G. D., Nelson, C. C., 2009, "Wind-US Code Enhancements to Complement Hypersonic Testing and Evaluation," AIAA Paper 2009-193.

[36]Engblom, W., Frate, F., and Nelson, C., 2005, "Progress in Validation of Wind-US for Ramjet/Scramjet Combustion," AIAA Paper 2005-1000.

[37]Lankford, D. W. and Nelson, C. C., 2002, "Application of the Wind Flow Solver to Chemically Reacting Flows," AIAA Paper 2002-673.

[38]Nelson, C. C., Cain, A. B., "Prediction of Store Trajectory Response to Unsteady Aerodynamic Loads," AIAA Paper 2009-548 (Invited), 2009.

[39]Nelson, C. C., Cain, A. B., Kerschen, E. J., and Raman, G., "Simulations of Helmholtz Resonator Powered Resonance Tubes at Moderate Pressure Ratios," AIAA Paper 2006-0800, 2006.

[40]Spalart, P. R., Jou, W.-H., Strelets, M., and Allmaras, S. R., "Comments on the Feasibility of LES for Wings and on a Hybrid RANS/LES Approach," *Advances in DNS/LES—Proceedings of the First AFOSR International Conference on DNS/LES*, 1997.

[41] Zdravkovich, M. M., "Review of Flow Interference Between Two Circular Cylinders in Various Arrangements," Journal of Fluids Engineering, Vol. 99, Dec. 1977, pp 618-633.